



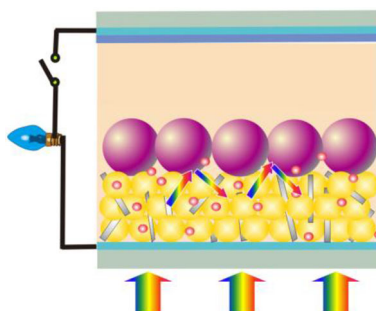
# A Bi-layer Composite Film Based on TiO<sub>2</sub> Hollow Spheres, P25, and Multi-walled Carbon Nanotubes for Efficient Photoanode of Dye-sensitized Solar Cell

Putao Zhang<sup>1,2</sup> · Zhiqiang Hu<sup>1</sup> · Yan Wang<sup>1</sup> · Yiyang Qin<sup>1</sup> · Wenqin Li<sup>2</sup> · Jinmin Wang<sup>2</sup>

Received: 29 November 2015 / Accepted: 15 December 2015 / Published online: 2 February 2016  
© The Author(s) 2016. This article is published with open access at Springerlink.com

**Abstract** A bi-layer photoanode for dye-sensitized solar cell (DSSC) was fabricated, in which TiO<sub>2</sub> hollow spheres (THSs) were designed as a scattering layer and P25/multi-walled carbon nanotubes (MWNTs) as an under-layer. The THSs were synthesized by a sacrifice template method and showed good light scattering ability as an over-layer of the photoanode. MWNTs were mixed with P25 to form an under-layer of the photoanode to improve the electron transmission ability of the photoanode. The power conversion efficiency of this kind of DSSC with bi-layer was enhanced to 5.13 %, which is 14.25 % higher than that of pure P25 DSSC.

**Graphical Abstract** A bi-layer composite photoanode based on P25/MWNTs-THSs with improved light scattering and electron transmission, which will provide a new insight into fabrication and structure design of highly efficient dye-sensitized solar cells.



**Keywords** Dye-sensitized solar cell · TiO<sub>2</sub> · Hollow spheres · Carbon nanotubes

✉ Zhiqiang Hu  
hzq@dlpu.edu.cn

✉ Jinmin Wang  
wangjinmin@sspu.edu.cn

<sup>1</sup> Institute of New Energy Material, Dalian Polytechnic University, Dalian 116034, People's Republic of China

<sup>2</sup> School of Environmental and Materials Engineering, College of Engineering, Shanghai Second Polytechnic University, Shanghai 201209, People's Republic of China

## 1 Introduction

In the past two decades, dye-sensitized solar cells (DSSCs) have attracted extensive attention due to their low cost, convenient fabrication, and less pollution to the environment [1, 2]. As one critical part of a DSSC, photoanode is usually made of nanocrystalline TiO<sub>2</sub> screen printed onto fluorine-doped tin oxide (FTO) substrate. A photoanode with high performance should have excellent light absorption ability and effective electron transmission

ability. However, these two features usually negate each other for single-layer nanocrystalline photoanode films. So, two or more layers of TiO<sub>2</sub> nanostructures are used to prepare complex nanocrystalline photoanodes, which is expected to having superior photovoltaic performance [3].

To improve the power conversion efficiency of DSSCs, researchers have made extensive efforts to modify the photoanodes [4–14]. In order to increase the absorption of sunlight and improve the photoelectric performance, scattering layers have been studied extensively. A variety of TiO<sub>2</sub> nanostructures [15–19] have been used as scattering layers. The introduction of these nanostructures increases the light propagation path in photoanodes, resulting in increased light absorption of DSSCs. Wang et al. prepared TiO<sub>2</sub> hollow spheres embedded with SnO<sub>2</sub> nanobeads as the scattering layer, which shows an efficient scattering effect [20]. Xiong et al. introduced titania films with hierarchical structure as scattering layers [21], and Shi et al. prepared hollow TiO<sub>2</sub> boxes as the scattering layer [22]. However, only increasing the absorption of light is not enough to improve the photovoltaic performance of DSSCs, researchers try to improve electronic transmission in photoanodes to improve the photovoltaic performance of DSSCs. One-dimensional (1D) TiO<sub>2</sub> nanostructures such as nanorods, nanowires, nanobelts, and nanotubes have been used in photoanodes with excellent electron transport ability [23–30]. Although the introduction of 1D TiO<sub>2</sub> nanostructures accelerates the electron transmission, the absorption of light is not improved at the same time. Hence, both electron transmission and light absorption should be considered to achieve a high-performance DSSC.

In this work, for light absorption, TiO<sub>2</sub> hollow spheres were synthesized and used as the scattering layer; for electron transmission, multi-walled carbon nanotubes (MWNTs) were mixed with P25 and used as the under-layer. Thus, a bi-layer composite film containing TiO<sub>2</sub> hollow spheres (THSs), P25, and MWNTs were used as the photoanode of a DSSC, exhibiting improved power conversion efficiency.

## 2 Experimental Section

### 2.1 Materials

Ethanol,  $\alpha$ -terpineol, concentrated sulfuric acid, ethyl cellulose, acetylacetone, octylphenol polyoxyethylene ether (OP-10) emulsifiers, and tetrabutyl titanate (TBT) were purchased from Sinopharm Chemical Reagent Co. Ltd. and

used without any further purification. MWNTs were purchased from Shanghai Lark Chemical Technology Co. Ltd. P25 was purchased from Dalian Qiseguang Solar Technology Development Co. Ltd.

### 2.2 Synthesis of THSs

Monodisperse polystyrene (PS) spheres were used as a template, which were prepared via a boiling emulsifier-free emulsion polymerization according to previous work [31]. In a typical preparation procedure, 2.0 g of PS spheres were placed into 20 mL of concentrated sulfuric acid under vigorous magnetic stirring at 40 °C for 15 h. After centrifugation and washing with ethanol for three times, sulfonated polystyrene (sPS) spheres were formed. Then 1.0 mL of tetrabutyl titanate and 15 mL of ethanol were mixed, and 1.0 g of sPS spheres were put into this mixed solution under magnetic stirring at room temperature for 1 h. After centrifugation and drying at 60 °C for 12 h, sPS spheres were coated with tetrabutyl titanate (tPS). The tPS spheres were calcined at 300 °C for 2 h in air to remove sPS spheres. To obtain THSs with the desired crystallinity, the powders were calcined in air at 500 °C for 30 min.

### 2.3 Pretreatment of MWNTs

MWNTs were pretreated with mixed acid according to previous work [32]. In a typical process, 0.5 g of MWNTs were oxidized in 80 mL of 1:3 (V:V) concentrated nitric acid–sulfuric acid mixed solution under ultrasonication at 60 °C for 10 h. Then, the MWNTs were separated by centrifugation and washed with distilled water several times until a final pH value of 6. The product was subsequently dried in a vacuum oven at 40 °C for 12 h.

### 2.4 Fabrication of DSSCs

For the preparation of the P25 paste, 1.0 g of P25, 10 mL of ethanol, 0.8 g of ethyl cellulose, 4.3 mL of  $\alpha$ -terpineol, 0.3 mL of acetylacetone, and 2 drops of OP-10 emulsifiers were mixed and grinded in an agate mortar for 1 h. THS paste and P25/MWNT paste (MWNTs, 0.1 wt%) were prepared by the same way [33]. To fabricate photoanodes, FTO-coated glasses were used as substrates, which were cleaned by sonication in acetone, deionized water, and ethanol each for 15 min, then blow dried with N<sub>2</sub>. TiO<sub>2</sub> films were prepared by screen printing method. The film thickness was controlled by screen printing times. The films were heated at 325, 375, and 425 °C each for 5 min,

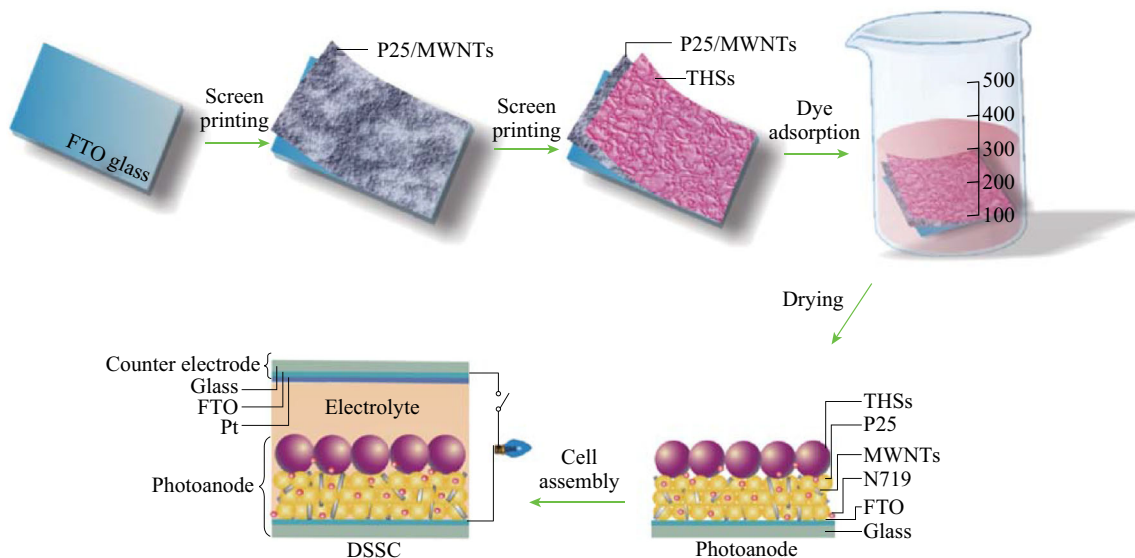


**Fig. 1** Schematic illustration for the preparation of P25/MWNTs-THSs DSSC

450 °C for 15 min, and at 500 °C for 30 min. After thermal treatment, the films were cooled down to 80 °C for dye sensitization for 24 h, then rinsed with ethanol and dried. The dye solution was 0.5 mmol L<sup>-1</sup> N719 acetonitrile/tertiary butanol (V/V = 1:1) solution. Counter electrodes were prepared by spin-coating of 0.02 mol L<sup>-1</sup> H<sub>2</sub>PtCl<sub>6</sub> isopropyl alcohol solution onto FTO glass, and then heating at 400 °C for 15 min. Finally, the sensitized photoanode was sealed together with the counter electrode, followed by the injection of electrolyte solution. The electrolyte solution is composed of 0.05 mol L<sup>-1</sup> I<sub>2</sub>, 0.10 mol L<sup>-1</sup> LiI, 0.60 mol L<sup>-1</sup> N-methyl-N-butyl imidazolium iodide (BMII), and 0.50 mol L<sup>-1</sup> 4-tert-butylpyridine (TBP) in acetonitrile. The fabrication process of the photoanode is illustrated in Fig. 1.

### 3 Characterization

The morphology of the sample was observed by field-emission scanning electron microscopy (FESEM, S-4800; Shimadzu Corporation). X-ray diffraction (XRD) pattern was used to study the crystal structure of the samples, using Cu K<sub>α</sub> (λ = 0.15418 nm) radiation in the 2θ range from 10° to 70° with a scanning speed of 10° min<sup>-1</sup>. The UV–Visible absorption spectrum was obtained by a UV–Visible spectrophotometer (UV-2600, Shimadzu Corporation). The current–voltage (*J*–*V*) characteristics and electrochemical impedance spectra (EIS) of the DSSCs were measured by an electrochemical workstation (Autolab, PGSTAT302 N,

Metrohm) under a light source for AM 1.5 radiation (Sun 2000 Solar Simulator, Abet Technologies).

### 4 Results and Discussion

Figure 2 shows the FESEM images of PS spheres, sulfonated PS spheres, PS spheres coated by tetrabutyl titanate, THSs, and the TEM image of a single THS. It can be seen from Fig. 2a that the well-dispersed PS spheres with a uniform diameter of ~250 nm and smooth surface were synthesized. After being sulfonated by concentrated sulfuric acid, the PS spheres were converted to sPS (Fig. 2b). Obviously, the surface of sPS is rougher than that of PS and the shape of sPS turns into irregular spheres. We can see some sPS spheres adhering together. Using tetrabutyl titanate (TBT) as a titania precursor to coat the sPS, the result shows that TBT is easily adsorbed onto the surface of sPS because of containing a large number of negative ions. The surface of tetrabutyl titanate-coated sPS spheres (with a diameter of ~300 nm) is very rough. From Fig. 2d, we can see that some broken THSs, which indicates that the template has been successfully removed. We can obtain the outer diameters and wall thickness of the THS from Fig. 2e. The two adjacent broken THSs have a two-wall thickness of ~50 nm, so the wall thickness of a THS is ~25 nm. The TEM image of a single THS (Fig. 2f) further confirms the existence of hollow cavity in the as-prepared product. The measured wall thickness is ~25 nm, and

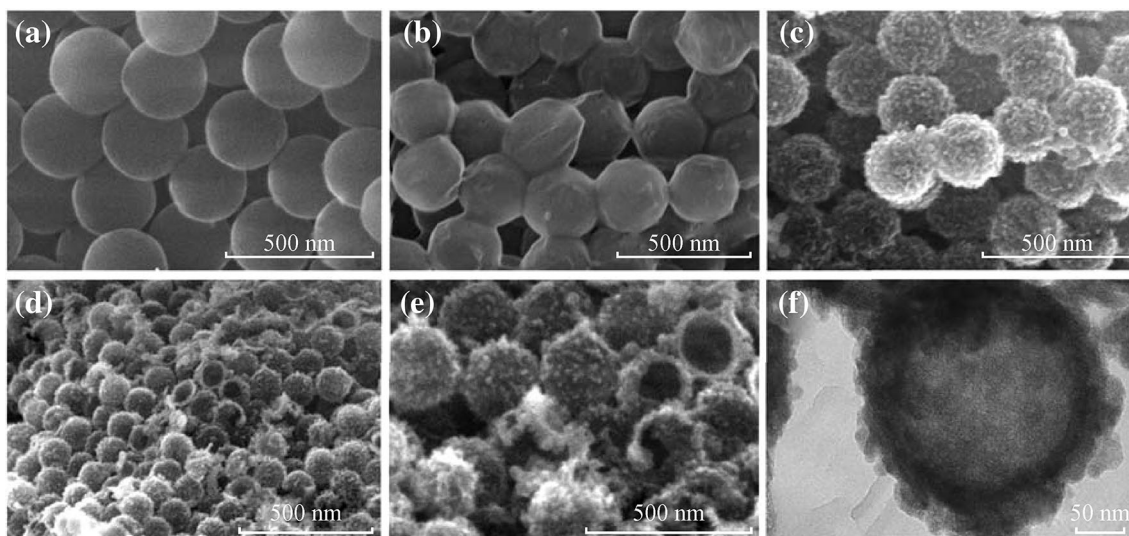


**Fig. 2** FESEM images of **a** PS, **b** sulfonated PS, **c** PS coated by tetrabutyl titanate, and **d**, **e** THSs, and **f** TEM image of a single THS

the surface is very rough. This corresponds well with the FESEM observations.

The XRD pattern of the as-prepared THSs is shown in Fig. 3. All the sharp peaks are in good agreement with the standard card of anatase  $\text{TiO}_2$  (JCPDS No. 21-1272). The sample is well crystalline and without any other impurities.

Figure 4a shows the cross-sectional FESEM image of the P25/MWNTs-THSs bi-layer film. It is seen that the thickness of the under-layer and the scattering layer is  $\sim 15$  and  $\sim 8 \mu\text{m}$ , respectively. Under high magnification, the scattering layer (see Fig. 4b) and the under-layer (see Fig. 4c) can be observed more clearly. The scattering layer containing THSs is composed of a disordered macroporous network, and these macropores in the scattering layer can enhance the absorption of light and the transfer of electrolyte [34–36]. The under-layer consisting of P25 and MWNTs can be seen in Fig. 4c. Some MWNTs are embedded in P25, which can enhance the electron transport of photoanode [32].

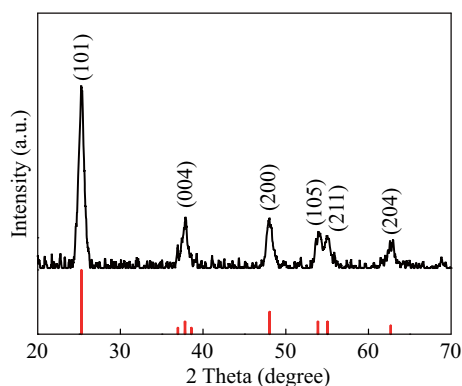


**Fig. 3** XRD pattern of the as-prepared THSs at 500 °C for 30 min

The dye molecules were desorbed from the dye-sensitized photoanodes of P25, P25/MWNTs, P25-THSs, and P25/MWNTs-THSs, and the corresponding UV–Vis absorbance spectra are shown in Fig. 5a. From these spectra, it can be seen that the absorbance of dye desorbed from the P25/THSs photoanode is higher than that of other photoanodes, P25 and P25/MWNTs-THSs nearly equal, and P25/MWNTs slightly lower. The specific values of dye molecules adsorbed in photoanodes can be calculated, the calculated amounts of desorbed dye are  $1.53 \times 10^{-7}$ ,  $1.23 \times 10^{-7}$ ,  $1.16 \times 10^{-7}$ , and  $1.03 \times 10^{-7} \text{ mol cm}^{-2}$  for P25-THSs, P25, P25/MWNTs-THSs, and P25/MWNTs photoanodes, respectively. The N719 dye was desorbed from the  $\text{TiO}_2$  films with  $0.2 \text{ mol L}^{-1}$  NaOH aqueous solution (5 mL), and the UV–Vis absorption spectra (Fig. 5a) of the obtained solution were measured. The concentration of N719 in NaOH aqueous solution ( $c$ ) can be calculated by the equation  $A = Kcl$ , where  $l$  is the path length of the light beam,  $K$  is the molar extinction coefficient of N719 at 515 nm, and  $A$  is the intensity of UV–Vis absorption spectra at 515 nm [37]. The obtained concentration multiplied by the volume of NaOH aqueous solution is equal to the amount of adsorbed N719, thus dye adsorption densities can be obtained accordingly. Figure 5b shows the absorption spectra of dye-sensitized films. Compared with the films of P25 and P25/MWNTs, P25-THSs and P25/MWNTs-THSs films have better absorption capacity in the wavelength range from 420 to 550 nm, which can be ascribed to the introduction of THSs as the scattering layer, and more light is reflected from the THSs layer and re-adsorbed by the under-layer. The films of P25/MWNTs and P25/MWNTs-THSs show enhanced absorption at higher range ( $>550 \text{ nm}$ ), because MWNTs can absorb some sunlight [38].



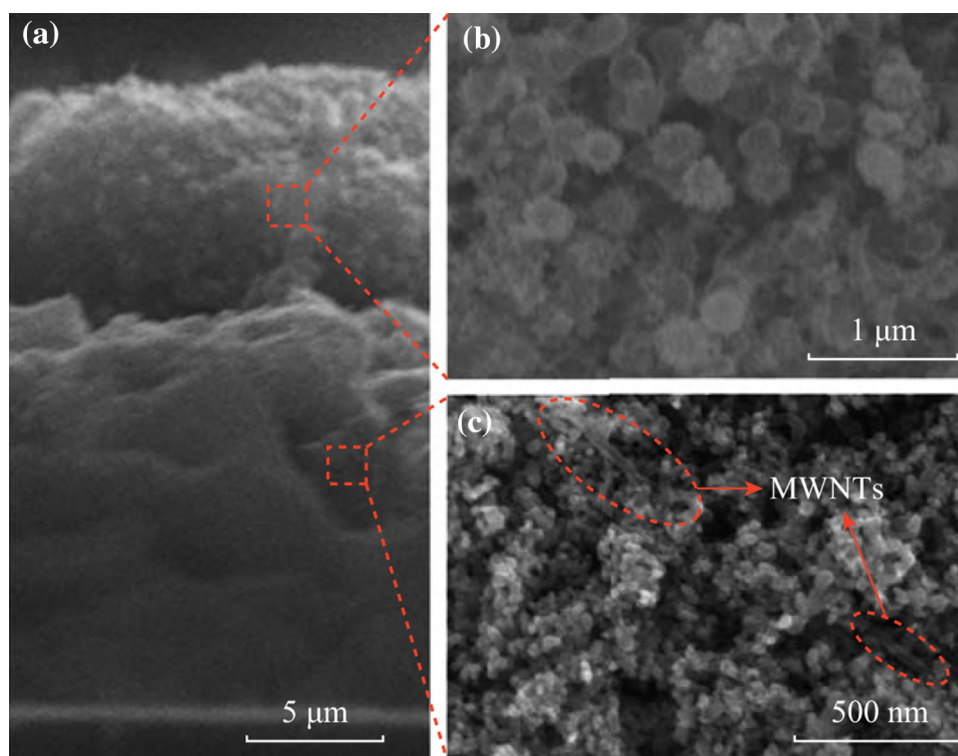


**Fig. 4** FESEM images of **a** cross section, **b** scattering layer containing THSs, and **c** under-layer containing P25/MWNTs

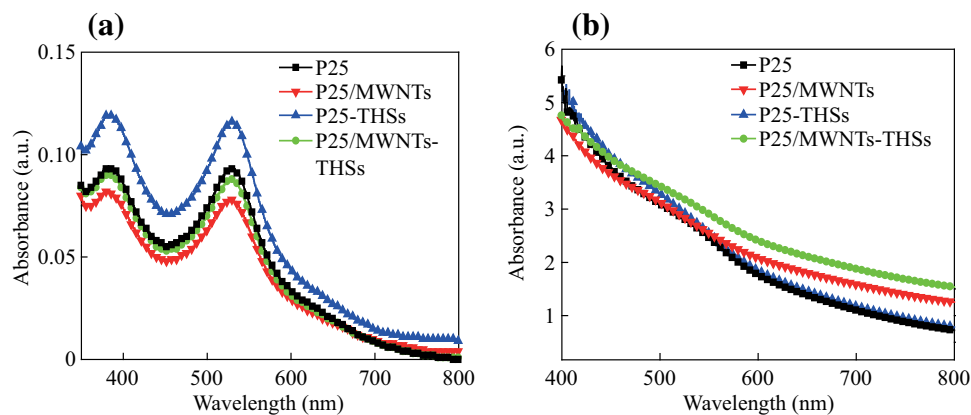


**Fig. 5** Absorption spectra of dye molecules desorbed from the dye-sensitized photoanodes **(a)** and absorption spectra of dye-sensitized films **(b)** of P25, P25/MWNTs, P25-THSs, and P25/MWNTs-THSs

Performances of DSSCs with the four kinds of photoanodes are examined under one sun AM 1.5 radiation simulated sunlight. Figure 6 presents the  $J$ - $V$  curves for the four kinds of solar cells. The corresponding photovoltaic parameters are summarized in Table 1. The DSSCs assembled with P25/MWNTs-THSs photoanode obtain an open voltage ( $V_{oc}$ ) of 0.72 V, a short circuit density ( $J_{sc}$ ) of  $11.31 \text{ mA cm}^{-2}$ , a fill factor ( $FF$ ) of 0.63, and a conversion efficiency ( $\eta$ ) of 5.13 %. It is interesting to note that  $J_{sc}$  and  $\eta$  vary significantly from 9.63 (pure P25) to  $11.31 \text{ mA cm}^{-2}$  (P25/MWNTs-THSs), and 4.49 (pure

P25) to 5.13 % (P25/MWNTs-THSs), respectively, compared to the DSSC based on pure P25 photoanode. The highly improved  $J_{sc}$  and  $\eta$  can be mainly attributed to two reasons: (a) the enhanced light harvesting due to the strong light scattering ability of THSs and (b) the improved electron transmission performance from the introduced MWNTs. The two reasons can be illustrated through comparing the photovoltaic properties of P25-THSs and P25/MWNTs solar cells with pure P25 solar cell. It is noted that the  $V_{oc}$  values (Table 1) of the four types of cells are not compatible with dye adsorption density.  $V_{oc}$  value is

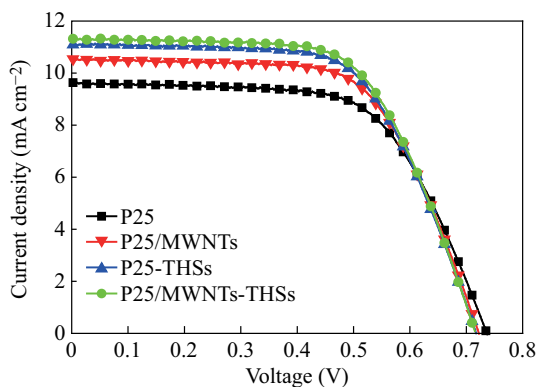


**Fig. 6** *J*–*V* curves of four kinds of DSSCs

**Table 1** Photovoltaic properties of DSSCs with different photoanodes

DSSC type	<i>V</i> <sub>oc</sub> (V)	<i>J</i> <sub>sc</sub> (mA cm <sup>−2</sup> )	<i>FF</i>	<i>η</i> (%)
P25	0.74	9.63	0.63	4.49
P25/MWNTs	0.73	10.54	0.63	4.85
P25-THSs	0.72	11.08	0.62	4.95
P25/MWNTs-THSs	0.72	11.31	0.63	5.13

determined by many factors, such as recombination resistance, dye adsorption density, and surface morphology of nanocrystalline photoanode [39, 40]. As shown in Fig. 7a,

when P25 nanoparticles and THSs are used as the under-layer and over-layer, respectively, the THSs play a key role in increasing the light scattering. More light is reflected from the THSs layer and re-adsorbed by P25 nanoparticle layer, which is beneficial to light harvesting and improving the power conversion efficiency of DSSCs ( $\eta_{P25} = 4.49\%$ ,  $\eta_{P25-THSs} = 4.95\%$ ). As shown in Fig. 7b, composite photoanode based on P25/MWNTs, due to the direct transport pathways provided by MWNTs, the electron transport rate is increased, and hence the charge recombination is reduced to some extent. This is also one of the factors to improve the power conversion efficiency of DSSCs ( $\eta_{P25} = 4.49\%$ ,  $\eta_{P25/MWNTs} = 4.85\%$ ). When putting THSs and MWNTs together into one photoanode, it exhibits an improved power conversion efficiency ( $\eta = 5.13\%$ ).

To deeply understand the effect of THSs and MWNTs on the performance of DSSCs, and hence reveal the electron transport within the DSSCs, electrochemical impedance spectroscopy (EIS) is further studied. EIS spectra of the four kinds of cells were observed under the illumination of one sun (AM 1.5, 100 mW cm<sup>−2</sup>) at the open circuit. The results of four samples are shown in the Nyquist plots (Fig. 8a) and the Bode curves (Fig. 8b). From Fig. 8a, we can see that the spectra are composed of two semicircles situated in high and middle frequency regimes. The small semicircle in the high-frequency region is related to charge

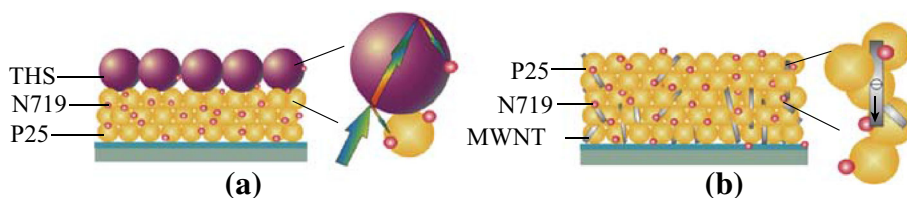


**Fig. 7** Schematic illustration of photoanodes based on (a) P25-THSs and (b) P25/MWNTs, showing different light scattering and electron transport effects

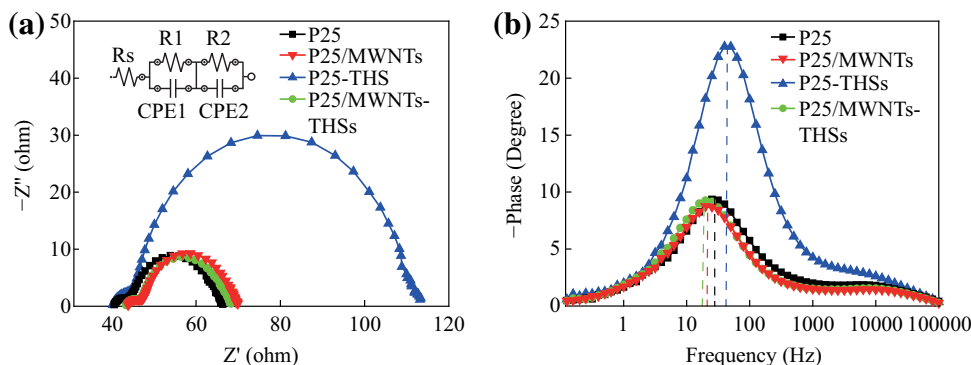


**Fig. 8** a Nyquist plot and b Bolt plot of DSSCs based on P25, P25/MWNTs, P25-THSs, and P25/MWNTs-THSs photoanodes. The inset in Fig. 8a displays the equivalent circuit model

**Table 2** EIS parameters of the DSSCs determined by fitting the experimental data to the equivalent circuit

DSSC types	$R_s$ ( $\Omega$ )	$R_1$ ( $\Omega$ )	$R_2$ ( $\Omega$ )	$\tau_c$ (ms)
P25	40.56	4.62	21.06	5.49
P25/MWNTs	43.36	4.46	20.46	8.85
P25-THSs	40.28	4.89	68.18	3.79
P25/MWNTs-THSs	43.88	4.07	22.01	7.96

transfer resistance ( $R_1$ ) and constant phase element (CPE1) at the electrolyte/Pt counter electrode interface. The large semicircle in the middle frequency region is related to recombination resistance ( $R_2$ ) and constant phase element (CPE2) at the  $\text{TiO}_2$ /dye/electrolyte interface. The inset of Fig. 8a is an equivalent circuit model, and the specific data of each element are listed in Table 2. We can see obviously that  $R_1$  is changed slightly and  $R_2$  shows a great difference.  $R_1$  is changed slightly because the four kinds of cells use the same Pt counter electrode and the same electrolyte, and  $R_1$  is related to the charge transfer at the interface between the electrolyte and the counter electrode. For recombination resistance,  $R_2$  noticeably increases (from 21.06 to 68.18  $\Omega$  for P25 and P25-THSs) when THSs are introduced into the photoanode as a scattering layer. The largest  $R_2$  for P25-THSs is due to the highest dye adsorption density of P25-THSs. From the Bode phase plots of EIS spectra (Fig. 8b), we can obtain information on electron lifetime ( $\tau_c$ ), and the specific data of  $\tau_c$  could be estimated from the equation  $\tau_c = 1/2\pi f$ , where  $f$  represents the characteristic frequencies of the maximum phase shift. As shown in Table 2, the  $\tau_c$  of P25/MWNTs and P25/MWNTs-THSs DSSCs is 8.85 and 7.96 ms, respectively, which has been improved than for the DSSC without MWNTs under the same conditions. It should be a consequence of MWNTs providing a direct pathway for electron transport.

## 5 Conclusions

In summary, anatase THSs have been synthesized through a simple sacrifice template method. THSs, P25, and MWNTs were used in a composite photoanode. THSs were used as the scattering layer in the photoanode, enhancing the light harvesting; P25 mixed with MWNTs was used as the under-layer in the photoanode, not only absorbing dye molecules but also providing a rapid pathway for electron transfer. DSSC based on such a composite photoanode achieves an improved power conversion efficiency of 5.13 %, which is 14.25 % higher than that of P25-based DSSC (4.49 %). This composite photoanode will provide a new insight into the fabrication and structure design of highly efficient DSSCs.

**Acknowledgments** We would like to acknowledge the support provided by the National High Technology Research and Development Program 863 (No. 2006AA05Z417), Science and Technology Platform Construction Project of Dalian (2010-354), the Program for Professor of Special Appointment (Eastern Scholar) at Shanghai Institutions of Higher Learning (No. 2013-70), “Shu Guang” project supported by Shanghai Municipal Education Commission and Shanghai Education Development Foundation (No. 13SG55), National Natural Science Foundation of China (NSFC) (No. 61376009), Science and Technology Commission of Shanghai Municipality (No. 14YF1410500), and Shanghai Young Teacher Supporting Foundation (No. ZZEGD14011).

**Open Access** This article is distributed under the terms of the Creative Commons Attribution 4.0 International License (<http://creativecommons.org/licenses/by/4.0/>), which permits unrestricted use, distribution, and reproduction in any medium, provided you give appropriate credit to the original author(s) and the source, provide a link to the Creative Commons license, and indicate if changes were made.

## References

1. B. O'regan, M. Grätzel, A low-cost, high-efficiency solar cell based on dye-sensitized colloidal  $\text{TiO}_2$  film. *Nature* **353**(6346), 737–740 (1991). doi:10.1038/353737a0
2. M. Grätzel, Photoelectrochemical cells. *Nature* **414**(6861), 338–344 (2001). doi:10.1038/35104607
3. K.J. Hwang, D.W. Park, S. Jin, S.O. Kang, D.W. Cho, Influence of dye-concentration on the light-scattering effect in dye-sensitized solar cell. *Mater. Chem. Phys.* **149**, 594–600 (2015). doi:10.1016/j.matchemphys.2014.11.013
4. M.Y. Gao, Y.C. Rui, H.Z. Wang, Y.G. Li, Q.H. Zhang, Submicrometer/nano bimodal  $\text{TiO}_2$  particles as easily sintered, crack-free, and current-contributed scattering layers for dye-sensitized solar cells. *J. Phys. Chem. C* **118**(30), 16951–16958 (2014). doi:10.1021/jp500466s
5. J.M. Wang, X.W. Sun, Z.H. Jiao, E. Khoo, P.S. Lee, J. Ma, H.V. Demir, Tailoring insoluble nanobelts into soluble anti-UV nanopotpourris. *Nanoscale* **3**(11), 4742–4745 (2011). doi:10.1039/c1nr10979k
6. E. Guo, L. Yin, Nitrogen doped  $\text{TiO}_2$ - $\text{Cu}_x\text{O}$  core-shell mesoporous spherical hybrids for high-performance dye-sensitized solar cell. *Phys. Chem. Chem. Phys.* **17**(1), 563–574 (2014). doi:10.1039/c4cp03132f
7. A.G. Vega-Poot, M. Macías-Montero, J. Idígoras, A. Borrás, A. Barranco, A.R. Gonzalez-Elipe, F.I. Lizama-Tzec, G. Oskam, J.A. Anta, Mechanisms of electron transport and recombination in  $\text{ZnO}$  nanostructures for dye-sensitized solar cells. *Chem. Phys. Chem.* **15**(6), 1088–1097 (2014). doi:10.1002/cphc.201301068
8. J.B. Chang, C.H. Liu, J. Liu, Y.Y. Zhou, X. Gao, S.D. Wang, Green-chemistry compatible approach to  $\text{TiO}_2$ -supported PdAu bimetallic nanoparticles for solvent-free 1-Phenylethanol oxidation under mild conditions. *Nano-Micro Lett.* **7**(3), 307–315 (2015). doi:10.1007/s40820-015-0044-6
9. J. Huang, C. Xia, L. Cao, X. Zeng, Facile microwave hydrothermal synthesis of zinc oxide one-dimensional nanostructure with three-dimensional morphology. *Mater. Sci. Eng. B* **150**(3), 187–193 (2008). doi:10.1016/j.mseb.2008.05.014
10. K. Kakiage, T. Tokutome, S. Iwamoto, S. Kyomen, M. Hanya, Fabrication of a dye-sensitized solar cell containing a Mg-doped  $\text{TiO}_2$  electrode and a  $\text{Br}^-/\text{Br}^-$ -redox mediator with a high open-circuit photovoltage of 1.21 V. *Chem. Commun.* **49**(2), 179–180 (2013). doi:10.1039/C2CC36873K

11. P.Z. Yang, Q.W. Tang, B.L. He, Toward elevated light harvesting: efficient dye-sensitized solar cells with titanium dioxide/silica photoanodes. *RSC Adv.* **5**(57), 46260–46266 (2015). doi:[10.1039/C5RA06584D](https://doi.org/10.1039/C5RA06584D)
12. Y. Wang, J. Zhai, Y. Song, Feather-like Ag@TiO<sub>2</sub> nanostructures as plasmonic antenna to enhance optoelectronic performance. *Phys. Chem. Chem. Phys.* **7**(17), 5051–5056 (2015). doi:[10.1039/C4CP05398B](https://doi.org/10.1039/C4CP05398B)
13. X.W. Li, Y.Q. Jiang, W.J. Cheng, Y.D. Li, X.Z. Xu, K.F. Lin, Mesoporous TiO<sub>2</sub>/carbon beads: one-pot preparation and their application in visible-light-induced photodegradation. *Nano-Micro Lett.* **7**(3), 243–254 (2015). doi:[10.1007/s40820-015-0029-5](https://doi.org/10.1007/s40820-015-0029-5)
14. J.M. Wang, L. Zhang, L. Yu, Z.H. Jiao, H.Q. Xie, X.W. Lou, X.W. Sun, A bi-functional device for self-powered electrochromic window and self-rechargeable transparent battery applications. *Nat. Commun.* **5**, 4921 (2014). doi:[10.1038/ncomms5921](https://doi.org/10.1038/ncomms5921)
15. Y.J. Kim, M.H. Lee, H.J. Kim, G. Lim, Y.S. Choi, N.G. Park, K.K. Kim, W.I. Lee, Formation of highly efficient dye-sensitized solar cells by hierarchical pore generation with nanoporous TiO<sub>2</sub> spheres. *Adv. Mater.* **21**(36), 3668–3673 (2009). doi:[10.1002/adma.200900294](https://doi.org/10.1002/adma.200900294)
16. C.S. Chou, M.G. Guo, K.H. Liu, Y.S. Chen, Preparation of TiO<sub>2</sub> particles and their applications in the light scattering layer of a dye-sensitized solar cell. *Appl. Energ.* **92**(4), 224–233 (2012). doi:[10.1016/j.apenergy.2011.10.038](https://doi.org/10.1016/j.apenergy.2011.10.038)
17. W.Q. Wu, Y.F. Xu, H.S. Rao, C.Y. Su, D.B. Kuang, A double layered TiO<sub>2</sub> photoanode consisting of hierarchical flowers and nanoparticles for high-efficiency dye-sensitized solar cells. *Nanoscale* **5**(10), 4362–4369 (2013). doi:[10.1039/c3nr00508a](https://doi.org/10.1039/c3nr00508a)
18. B. Wang, P. Sun, F. Liu, Bilayered photoanode from rutile TiO<sub>2</sub> nanorods and hierarchical anatase TiO<sub>2</sub> hollow spheres: a candidate for enhanced efficiency dye sensitized solar cells. *RSC Adv.* **4**(110), 64737–64743 (2014). doi:[10.1039/C4RA11895B](https://doi.org/10.1039/C4RA11895B)
19. G.T. Dai, L. Zhao, J. Li, L. Wan, F. Hu et al., A novel photoanode architecture of dye-sensitized solar cells based on TiO<sub>2</sub> hollow sphere/nanorod array double-layer film. *J. Colloid Interf. Sci.* **365**(1), 46–52 (2012). doi:[10.1016/j.jcis.2011.08.073](https://doi.org/10.1016/j.jcis.2011.08.073)
20. C.L. Wang, J.Y. Liao, Y. Zhao, A. Manthiram, Template-free TiO<sub>2</sub> hollow microspheres embedded with SnO<sub>2</sub> nanobeads as a versatile scattering layer for dye-sensitized solar cells. *Chem. Commun.* **51**(14), 2848–2850 (2015). doi:[10.1039/C4CC07700H](https://doi.org/10.1039/C4CC07700H)
21. Y. Xiong, D. He, Y. Jin, P.J. Cameron, K.J. Edler, Ordered mesoporous particles in titania films with hierarchical structure as scattering layers in dye-sensitized solar cells. *J. Phys. Chem. C* **119**(39), 22552–22559 (2015). doi:[10.1021/acs.jpcc.5b06977](https://doi.org/10.1021/acs.jpcc.5b06977)
22. J. Feng, Y. Hong, J. Zhang, P. Wang, Z. Hu, Q. Wang, L. Hanb, Y. Zhu, Novel core-shell TiO<sub>2</sub> microsphere scattering layer for dye-sensitized solar cells. *J. Mater. Chem. A* **2**(5), 1502–1508 (2014). doi:[10.1039/C3TA13523C](https://doi.org/10.1039/C3TA13523C)
23. B. Liu, E.S. Aydil, Growth of oriented single-crystalline rutile TiO<sub>2</sub> nanorods on transparent conducting substrates for dye-sensitized solar cells. *J. Am. Chem. Soc.* **131**(11), 3985–3990 (2009). doi:[10.1021/ja8078972](https://doi.org/10.1021/ja8078972)
24. B.H. Lee, M.Y. Song, S.Y. Jang, S.M. Jo, S.Y. Kwak, D.Y. Kim, Charge transport characteristics of high efficiency dye-sensitized solar cells based on electrospun TiO<sub>2</sub> nanorod photoelectrodes. *J. Phys. Chem. C* **113**(51), 21453–21457 (2009). doi:[10.1021/jp907855x](https://doi.org/10.1021/jp907855x)
25. W.Q. Wu, B.X. Lei, H.S. Rao, Y.F. Xu, Y.F. Wang, C.Y. Su, D.B. Kuang, Hydrothermal fabrication of hierarchically anatase TiO<sub>2</sub> nanowire arrays on FTO Glass for dye-sensitized solar cells. *Sci. Rep.* **3**(13), 1352–1358 (2013). doi:[10.1038/srep01352](https://doi.org/10.1038/srep01352)
26. M. Yu, Y.Z. Long, B. Sun, Z.Y. Fan, Recent advances in solar cells based on one-dimensional nanostructure arrays. *Nanoscale* **4**(9), 2783–2796 (2012). doi:[10.1039/c2nr30437f](https://doi.org/10.1039/c2nr30437f)
27. M.D. Ye, X.K. Xin, C.J. Lin, Z.Q. Lin, High efficiency dye-sensitized solar cells based on hierarchically structured nanotubes. *Nano Lett.* **11**(8), 3214–3220 (2011). doi:[10.1021/nl2014845](https://doi.org/10.1021/nl2014845)
28. J.M. Wang, E. Khoo, P.S. Lee, J. Ma, Synthesis, assembly and electrochromic properties of uniform crystalline WO<sub>3</sub> nanorods. *J. Phys. Chem. C* **112**(37), 14306–14312 (2008). doi:[10.1021/jp804035r](https://doi.org/10.1021/jp804035r)
29. F.D.S. Fonzo, A.L. Bassi, C.S. Casari, V. Russo, G. Divitini, C. Ducati, E.C. Bottani, P. Comte, M. Grätzel, Hierarchical TiO<sub>2</sub> photoanode for dye-sensitized solar cells. *Nano Lett.* **10**(7), 2562–2567 (2010). doi:[10.1021/nl101198b](https://doi.org/10.1021/nl101198b)
30. X.T.E. Ashalley, F. Lin, H.D. Li, Z.M. Wang, Advances in MoS<sub>2</sub>-based field effect transistors (FETs). *Nano-Micro Lett.* **7**(3), 203–218 (2015). doi:[10.1007/s40820-015-0034-8](https://doi.org/10.1007/s40820-015-0034-8)
31. C. Chen, Z.G. Zhu, W.H. Shi, Q.Q. Ge, M.J. Liu, X.R. Zhu, Facile preparation and self-assembly of monodisperse polystyrene nanospheres for photonic crystals. *J. Nanosci. Nanotechnol.* **15**(4), 3239–3243 (2015). doi:[10.1166/jnn.2015.9631](https://doi.org/10.1166/jnn.2015.9631)
32. J.G. Yu, J.J. Fan, B. Cheng, Dye-sensitized solar cells based on anatase TiO<sub>2</sub> hollow spheres/carbon nanotube composite films. *J. Power Sour.* **196**(18), 7891–7898 (2011). doi:[10.1016/j.jpowsour.2011.05.014](https://doi.org/10.1016/j.jpowsour.2011.05.014)
33. S.W. Zhang, H.H. Niu, Y. Lan, C. Cheng, J.Z. Xu, X.K. Wang, Synthesis of TiO<sub>2</sub> nanoparticles on plasma-treated carbon nanotubes and its application in photoanodes of dye-sensitized solar cells. *J. Phys. Chem. C* **115**(44), 22025–22034 (2011). doi:[10.1021/jp206267x](https://doi.org/10.1021/jp206267x)
34. X.X. Yu, J.G. Yu, B. Cheng, B.B. Huang, One-pot template-free synthesis of monodisperse zinc sulfide hollow spheres and their photocatalytic properties. *Chem. Eur. J.* **15**(27), 6731–6739 (2009). doi:[10.1002/chem.200900204](https://doi.org/10.1002/chem.200900204)
35. J.G. Yu, Q.L. Li, Z. Shu, Dye-sensitized solar cells based on double-layered TiO<sub>2</sub> composite films and enhanced photovoltaic performance. *Electrochim. Acta* **56**(18), 6293–6298 (2011). doi:[10.1016/j.electacta.2011.05.045](https://doi.org/10.1016/j.electacta.2011.05.045)
36. L. Yang, Y. Lin, J. Jia, X. Xiao, X. Li, X. Zhou, Light harvesting enhancement for dye-sensitized solar cells by novel anode containing cauliflower-like TiO<sub>2</sub> spheres. *J. Power Sour.* **182**(1), 370–376 (2008). doi:[10.1016/j.jpowsour.2008.03.013](https://doi.org/10.1016/j.jpowsour.2008.03.013)
37. I. Jang, T. Kang, W. Cho, Y.S. Kang, S.-G. Oh, S.S. Im, Preparation of silver nanowires coated with TiO<sub>2</sub> using chemical binder and their applications as photoanodes in dye sensitized solar cell. *J. Phys. Chem. Solids* **86**(7), 122–130 (2015). doi:[10.1016/j.jpcs.2015.07.005](https://doi.org/10.1016/j.jpcs.2015.07.005)
38. K.T. Dembele, R. Nechache, L. Nikolova, A. Vomiero, C. Santato, S. Licoccia, F. Rosei, Effect of multi-walled carbon nanotubes on the stability of dye sensitized solar cells. *J. Power Sour.* **233**(1), 93–97 (2013). doi:[10.1016/j.jpowsour.2013.01.075](https://doi.org/10.1016/j.jpowsour.2013.01.075)
39. Y.M. Feng, J.H. Zhu, J. Jiang, W.W. Wang, G.X. M, F. Wu, Building smart TiO<sub>2</sub> nanorod networks in/on the film of P25 nanoparticles for high-efficiency dye sensitized solar cells. *RSC Adv.* **4**(25), 12944–12949 (2014). doi:[10.1039/c3ra47869f](https://doi.org/10.1039/c3ra47869f)
40. L. Zhao, J. Li, Y. Shi, S. Wang, J. Hu, B. Dong, P. Wang, Double light-scattering layer film based on TiO<sub>2</sub> hollow spheres and TiO<sub>2</sub> nanosheets: improved efficiency in dye-sensitized solar cells. *J. Alloy. Compd.* **575**(28), 168–173 (2013). doi:[10.1016/j.jallcom.2013.02.045](https://doi.org/10.1016/j.jallcom.2013.02.045)